

Fermi Level Depinning in Two-Dimensional Materials Using a Fluorinated Bilayer Graphene Barrier

Cunzhi Sun^{§,†,‡}, Cheng Xiang^{†,‡}, Rongdun Hong[§], Feng Zhang[§], Timothy J. Booth^{†,‡}, Peter Bøggild^{†,‡,*}, and Manh-Ha Doan^{†,‡,*}

[§] Department of Physics, Xiamen University, Xiamen, 361005, P. R. China

[†] Department of Physics, Technical University of Denmark, Kgs. Lyngby 2800, Denmark

[‡] Centre for Nanostructured Graphene (CNG), Technical University of Denmark, Kgs. Lyngby 2800, Denmark

ABSTRACT: Strong Fermi level pinning (FLP) - often attributed to metal-induced gap states at the interfacial contacts - severely reduces the tunability of the Schottky barrier height of the junction and limits applications of the 2D materials in electronics and optoelectronics. Here, we show that fluorinated bilayer graphene (FBLG) can be used as a barrier to effectively prevent FLP at metal/2D materials interfaces. FBLG can be produced via short exposure (1-3 min) to SF₆ plasma that fluorinates only the top layer of a bilayer graphene with covalent C-F bonding, while the bottom layer remains intrinsic, resulting in a band gap opening of about 75 meV. Inserting FBLG between the metallic contacts and a layer of MoS₂ reduces the Schottky barrier height dramatically for the low-work function metals (313 and 260 meV for Ti and Cr, respectively) while it increases for the high-work function one (160 meV for Pd), corresponding to an improved pinning factor. Our results provide a straightforward method to generate atomically thin dielectrics with applications not only for depinning the Fermi level at metal/transition metal dichalcogenide (TMD) interfaces but also for solving many other problems in electronics and optoelectronics.

KEY WORDS: *bilayer graphene, band gap opening, 2D materials, Fermi level pinning, Schottky barrier*

INTRODUCTION

As the number of transistors per CPU has increased exponentially in the last decades, a trend known as Moore's law, various challenges are emerging in the conventional silicon semiconductor technology when the transistor is scaled down to sub-10 nanometers^{1,2}. Two-dimensional (2D) materials, such as graphene and transition-metal dichalcogenides (TMDs), have drawn tremendous attention recently due to their promising advantages including atomic thickness and smooth channel-to-dielectric interface without dangling bonds^{3,4}. However, while the absence of bandgap in graphene results in a high off-current of the device, a high contact resistance of metal/TMD junctions makes it difficult to inject charge carriers to the channel^{5,6}. Opening a bandgap of graphene and reducing the contact resistance of TMDs, therefore, are the important directions to bring these materials to pragmatic switching applications.

Strong Fermi level pinning (FLP) is generally observed in metallic contacts to the 2D materials, originating from metal-induced gap states at the interface⁷⁻⁹. This renders the Schottky barrier height (SBH) of the junction uncontrollable and leads to increase of the contact resistance¹⁰. Traditionally, doping semiconductors at the contact region and/or using a metal-insulator-semiconductor structure can release the FLP and allow for an ohmic contact^{11,12}. Since strong, highly local doping of 2D materials is not yet a practical route to solving the problem, insertion of a buffer layer between the metal contact and TMDs is considered an effective alternative way to alleviate the FLP⁸⁻¹⁰. Indeed, by insertion of a thin insulating layer, such as TiO₂, ZnO, or h-BN at the metal/MoS₂ interfaces, the SBH can be significantly reduced, improving the pinning factor and the contact resistance¹³⁻¹⁵. The thickness of the insulator should be carefully controlled, since a thick layer would block the FLP but also increase the tunneling resistance. Using graphene as an interlayer could help to reduce the SBH at the metal/TMD interface but does not alleviate the FLP because graphene itself is a (semi)metal. It has been reported that strong fluorinating agents, namely xenon difluoride (XeF₂), can turn monolayer graphene to an insulator with a band gap of 3 eV due to formation of sp² C-F bonding on both sides, creating fluorographene¹⁶. However, stacking the double-side fluorinated graphene monolayer on a TMD will not result in smooth and stable contacts due to the covalent bonding of F atoms at the graphene/TMD interface.

In this study, we show that fluorinated bilayer graphene (FBLG) can be used as an interlayer to effectively prevent FLP at metal-2D material interfaces. Raman scattering and X-ray photoelectron

spectroscopy (XPS) measurements reveal that after 1-3 minutes of exposure to SF₆ plasma only the top layer of bilayer graphene is fluorinated with covalent C-F bonds, while the bottom layer remains intrinsic and free of dangling bonds and F species. Fluorination of mono- and bilayer graphene has previously been observed to lead to opening of a bandgap in the BLG¹⁷. As a proof of concept, we fabricate and investigate the transport properties of metal/FBLG-contacted MoS₂ transistors, using contact metals with different work functions. The extracted SBH in control devices without a FBLG layer at the metal/MoS₂ junctions is almost identical for all metals as characteristic for strong FLP. On insertion of FBLG, the SBH dramatically reduces for the low-work function metals, resulting in higher on-current of the transistor. In addition, it alleviates the line-up effect of the work function of the metal at the interface, leading to a better pinning factor. Our results define a straightforward method to generate thin dielectrics for depinning the Fermi level at metal/TMD interfaces in 2D material-based devices, as well as for various applications in advanced electronics and optoelectronics, and can be readily applied at the wafer scale using chemical vapor deposited graphene.

RESULTS AND DISCUSSION

To demonstrate a possible gap opening in FBLG, we fabricate field-effect transistors (FET) using exfoliated bilayer graphene on SiO₂/Si substrates both with and without applying the fluorination process, and investigate their electrical transport properties (Figure 1). BLG flakes were identified from the visual contrast in an optical microscope¹⁸ and verified by Raman scattering and atomic force microscopy (AFM) measurements. The samples were annealed at 300 °C in Ar/H₂ environment for 2 hours to remove residues on their surfaces. Fluorination is carried out in an inductively coupled plasma (ICP) etcher with SF₆ precursor gas under a high vacuum of 10⁻⁶ Torr over a typically short time (1-2 min) in attempt to limit fluorination to the top layer. To verify this, we used Raman spectroscopy and X-ray photoelectron spectroscopy (XPS) to examine the sample after fluorination. Figure 2a shows the evolution in the Raman spectrum of BLG with increasing fluorination time. Features corresponding to defect active bands are observed during fluorination, which include a blue-shift of the G peak, reduced intensity and broadened full width of half-maximum (FWHM) of the 2D peak, and the appearance of the D and D' peaks. Figure 2b shows the trends of the 2D peak as a function of fluorination time. The 2D peak of pristine BLG is well fitted by four Lorentzian components while after 185 seconds of fluorination it is best fitted with

only one component (see SI, Figure S1). This is attributed to a progressive transform of the 2D band of the bilayer into one of a monolayer. The enlarged FWHM of the 2D peak is due to loss of the AB-stacking configuration caused by induced-defects on the top graphene layer^{16,19,20}. It is also noted that the FWHM of the D peak in our fluorinated BLG is about 40 cm⁻¹ (see SI, Figure S1), which is in line with the previous studies on the Raman spectra of single-side functionalized BLG¹⁹. This indicates that only the top layer of BLG is fluorinated, while the bottom layer remains pristine, with C-F covalent bonds forming only on surface of the top layer of BLG, as illustrated Figure 1a.

Metal contacts of Cr/Au (20/80 nm) are made on pristine and fluorinated graphene using standard electron-beam lithography and e-beam evaporation²¹. The current-voltage characteristics of the BLG device shows a linear behavior with high conductivity, while it is nonlinear with much lower current in the FBLG device, as seen in Figure 1c. Using Si as a back-gate through the SiO₂ insulating layer, we clearly observe the distinctive features in the transfer curve of FBLG compared to that of pristine BLG including i) increased resistance (without, however, reaching the insulating regime as in the case of fluorographene¹⁶ or perfluorographene²⁰), ii) improved on-off ratio, and iii) a large 40 V shift of the charge-neutrality point towards the positive gate voltage. We attribute these effects to a small bandgap opening and p-doping in BLG after fluorination²²⁻²⁴.

The fluorination induces an asymmetry between the top and bottom graphene layers due to differences in carrier concentrations and/or a disordered lattice structure. Varying the back-gate voltage increases this inequivalence further. As a result, changes in the Coulomb potential lead to opening of a gap between valence and conduction bands of BLG²⁴. To estimate the electrical bandgap of FBLG, we adopt a well-known method built by Xia et al., which assumes that the off-current of the BLG transistor is proportional to $\exp(-q\phi_{\text{barrier}} / k_{\text{B}}T)$, where q is the electron charge, ϕ_{barrier} is the SBH at the interface of BLG and metal electrodes, k_{B} is the Boltzmann constant, and T is the temperature²⁵. The bandgap of BLG is double the size of the SBH at the charge neutrality point. Then, the increased bandgap of fluorinated BLG is as $\Delta E_{\text{g}} = 2\Delta(\phi_{\text{barrier}}) = 2(k_{\text{B}}T / q) \ln(I_{\text{off}}^0 / I_{\text{off}})$, where I_{off}^0 and I_{off} are the off-currents of pristine and fluorinated graphene, respectively. The bandgap of our FBLG is estimated to be about 75 meV, which is in a similar range of the molecular doped BLG reported in references 22 and 23.

Figure 3 presents the XPS spectra of BLG after 185 sec fluorination. In the C1s spectrum region (Figure 3a), beside the strong and sharp peak of the C-C sp² bond centered at about 284 eV, we

clearly observe the satellite peaks relating to the C-F bonds. The peak (red color) at about 285.2 eV correspond to the C-CF sp³ covalent bonds²⁶. The features at around (violet) 287, (blue) 290.7 (blue) and (green) 292 eV are attributed to the C-F_{2,3}, C-F₂ and C-F₃ groups, respectively^{26,27}. The relative amount of these components extracted from the fitting procedure is about 30%, 7.6%, 34%, and 3.6%, respectively. It should be noted that these amounts may not represent the exact fractions of the chemical groups on the sample due to the complexity of the surface chemistry of FBLG. This does, however, confirm the existence of the C-F bonds on the surface of BLG after fluorination. Figure 3b shows the XPS spectrum of the FBLG in the F1s region, confirming the co-existence of the covalent and so-called semi-ionic F-C bonds on FBLG²⁷.

Having established that the BLG is transformed into FBLG with a small bandgap, we now use it as an interlayer between metal contacts and semiconducting TMDs to investigate the Fermi level pinning effect. We choose MoS₂ as the conducting channel for the fabricated FET device, since this material is most intensively studied among TMDs with promising advantages for various applications in field-gated electronics²⁸, optoelectronics²⁹, spintronics³⁰, valleytronics³¹, sensors³² and so on³³. Multilayer MoS₂ with a thickness of about 10 nm is first mechanically exfoliated on a SiO₂/Si substrate using the scotch-tape method³⁴. BLG is produced by the mechanical exfoliation method and stacked on the MoS₂ flake by aligned transfer under a microscope^{34,35}. The sample then is coated by a polymethyl methacrylate (PMMA) layer, and the contact regions are opened by using the electron-beam lithography process. Fluorination is applied to induce FBLG, and metals with different work functions including Ti, Cr, Au, and Pd with a thickness of 20 nm are deposited as the electrical contacts. To protect the metals from oxidation, all the contacts are covered by a thick Au layer (100 nm). The channel region is defined by another lithography step, and the remaining excess BLG on MoS₂ is etched away using oxygen plasma, resulting in the FET structure shown in the inset of Figure 4a. Control devices, wherein the metal contacts are directly deposited on MoS₂ or using BLG without fluorination as the insertion layer, are fabricated under the same conditions to allow for a direct comparison. Figure 4 shows the gate-modulated currents (transfer curves) of the MoS₂ FET without and with the FBLG insertion layer. It is clearly observed that for low work function metals (Ti and Cr), much higher on-currents in all gate voltage regimes are achieved with insertion of the FBLG layer, while for high-work function metals (Au and Pd), there are crossover points in the transfer curves of the devices without and with FBLG. The increased current of the devices with Ti/FBLG and Cr/FBLG contacts is a result of the reduced

Schottky barrier height at the metal/MoS₂ junctions, and the crossover point is signature of the injection of holes into the valence band of MoS₂ [36].

To get the effective SBH at the metal contacts and MoS₂ interfaces, we adopt the 2D thermionic emission equation to extract the activation energy from the slope of an Arrhenius plot. At a certain temperature, current flow in the channel as^{7,9}

$$I_{2D} = WA_{2D}^* T^{3/2} \exp\left(\frac{q\phi_B}{k_B T}\right) \exp\left(\frac{qV_D}{k_B T}\right), \quad (1.1)$$

where W is the channel width, A_{2D}^* is the 2D equivalent Richardson constant, ϕ_B is the SBH, and V_D is the applied drain voltage. We measured transfer curves of the devices at different temperatures, and extracted SBH at each gate voltage by linearly fitting of the plot of $\ln(I/T^{3/2})$ versus $1000/T$. The extracted SBH, ϕ_B , is then plotted as a function of gate voltage for all devices as shown in Figure 5a-d. We applied $V_D = 1$ V to extract the SBH in all devices using comparable conditions. The use of a relatively high V_D contributes to reduce the impact of the Schottky barrier at the drain side⁷. The effective SBH at the contact junction is defined as the activation energy at the flat-band gate voltage, which is seen as the point where ϕ_B ceases to decrease linearly with gate voltage³⁷. It can be seen in Figure 5a-d that when the metals form direct contact to MoS₂, the SBH is just slightly changed (50 meV) from Ti to Pd, even though the difference of work function between these two metals is about 1 eV. This is clear evidence of the strong FLP effect at the metal/MoS₂ junctions. By insertion of FBLG, however, the SBH significantly reduces for the Ti and Cr electrodes, consistent with the increased current in the transfer curve above (Figure 4a, b). The reduction of the SBH in case of Au contact is small (Figure 5c), and interestingly, the SBH increases when FBLG is inserted between Pd and MoS₂ (Figure 5d).

Experimentally, strong Fermi level pinning observed in 2D material-based devices is usually attributed to several mechanisms including i) penetration of the wave function of metal contact electrons into the 2D crystal, which induces a large metal induced gap states (MIGS) even for an ideal 2D surface without defects^{9,10}, ii) intrinsic defects and/or impurities in 2D materials, and iii) extrinsic disorder-induced gap states (DIGS) forming during device processing⁷⁻¹⁰. Despite the surface of the TMD materials having no dangling bonds, a high density of intrinsic defects (10^{10} to 10^{11} per cm⁻²) is generally observed in thin flakes exfoliated from bulk materials due to presence of impurities, S-vacancies, and/or metal-like defects in the crystal^{38,39}. Moreover, deposition of the

contacts using an electron-beam evaporation process can introduce defects in the crystal structure of the TMD monolayers or topmost TMD layers, generating the extrinsic disorder-induced gap states⁴⁰. We anticipate that all these factors contribute to Fermi level pinning in our MoS₂ devices, although which mechanism is dominant is not clear or easy to determine. As a result, a large SBH forms at the interface, despite that the work function of Ti (4.3 eV) and Cr (4.5 eV) is above or aligned with the conduction band minimum of MoS₂. In addition, due to the strong FLP, the Fermi levels of the metals are lined-up and pinned to the MIGS, as illustrated in the inset of Figure 5f (left panel). Insertion of FBLG weakens the FLP owing to the two effects. It prevents the formation of MIGS since distance between the metal contact and MoS₂ surface is increased. In addition, FBLG acts as a protection layer to reduce the DIGS formed on the surface of MoS₂ in the contact region during metal deposition. These, consequently, reduces the band bending and removes the lining-up of the work functions of the metals, depicted in the inset of Figure 5f (right panel). Insertion of FBLG weakens the FLP owing to the two effects. It prevent the formation of MIGS since distance between the metal contact and MoS₂ surface is increased. In addition, FBLG acts as a protection layer to reduce the DIGS formed on the surface of MoS₂ in the contact region during metal deposition. These, consequently, alleviates the band bending and removes the line-up of the work function of the metal, depicted in the inset of Figure 5f (right panel). This explains the observation of the opposite trends in SBH of the contacts with low (Ti, Cr) and high (Pd) work functions, after FBLG insertion.

Ideally the SBH, ϕ_B , is given by the difference between the work function of a metal, ϕ_M , and the electron affinity of the semiconductor, χ , following the Schottky-Mott (SM) rule⁴¹

$$\phi_B = \phi_M - \chi \quad (1.2)$$

However, the MIGS formed at the interface produce deviations from the SM rule and introduces a Fermi level pinning effect. The SBH is then characterized quantitatively by introducing a pinning factor, S , and charge neutrality level, ϕ_{CNL} , as⁴¹

$$\phi_B = S(\phi_M - \phi_{\text{CNL}}) + (\phi_{\text{CNL}} - \chi) \quad (1.3)$$

The pinning factor is used to estimate how severely FLP occurs at the contacts. In the ideal case, $S = 1$ (the SM rule) where no FLP at the interface, while zero value of S represents complete pinning. Experimentally, S can be defined as the slope of ϕ_B vs. ϕ_M . Figure 5e shows the S values extracted from the MoS₂ devices with the different metal contacts without and with the FBLG

interlayer. It is obvious that S is typically small (0.07) when the metals directly contact MoS_2 , reconfirming strong FLP. We observe that insertion of pristine BLG makes FLP slightly more pronounced. The exact mechanism why pristine BLG leads to a smaller value of S is not clear at this point. Using fluorinated BLG as the interlayer, we would improve the pinning factor to more than 5 times to reach $S = 0.37$ (the red line). This value is even higher than those reported to date using high-quality thin insulating interface layers such as TiO_2 , ZnO , or h-BN ¹³⁻¹⁵. Figure 5f summarizes our observations of FLP in our MoS_2 devices using the different metal contacts without and with FBLG. Insertion of FBLG between the metal and MoS_2 results in a significant reduction in available MIGS, lowers the band banding of MoS_2 , alleviates the line-up of metal work function, and de-pins the Fermi level.

The pinning factor of our MoS_2 device with FBLG is about 0.37, which is still not close to the ideal case ($S = 1$), indicating that there some degree of Fermi level pinning is still remaining at the metal/FBLG / MoS_2 interface. This may be because the thickness and/or bandgap of FBLG is not sufficiently optimized. Further studies are being carried out to achieve even better results using CVD-grown graphene, where multiple transfers can be used to optimize the thickness in a practical and scalable manner. Since the fluorination anyway decouples the top-layer from the bottom layer, whether the BLG was initially Bernal stacked or not, the stacking order of the BLG is very likely not to have any influence on the result. This opens for the intriguing possibility of replacing BLG, which is still challenging to grow on a large scale, with two large, sequentially transferred single-layer graphene sheets grown by chemical vapor deposition. Wafer-scale growth and transfer techniques for graphene and other 2D materials have been developed rapidly in the recent years⁴²⁻⁴⁵ and are today mature routes for mass-production. Further study is needed to ultimately prove that non-Bernal stacked CVD graphene bilayers can indeed be used for large-scale de-pinning of the Fermi level of TMD devices and employed in mass production of 2D electronics.

CONCLUSION

In summary, our work demonstrates a simple and fast process to convert (semi)metallic BLG to the fluorinated bilayer graphene system where C-F bonds form only on the surface of the top graphene layer. This allows us to open a small bandgap of the top layer while keeping the bottom layer intrinsic and free of dangling bonds. We prove that this FBLG layer can be used as an interlayer between the metal contacts and MoS_2 to effectively prevent FLP, and thus reduce contact

resistance. Our result provides a new strategy to fabricate new synthetic 2D dielectrics that have the potential to be scaled effectively by replacing the BLG with double-transferred CVD-grown single layer graphene. This atomically thin layer has useful applications not only in de-pinning the Fermi level at metal/TMDs junctions in 2D materials devices, but also paves the way to various applications such as insulating protective coatings for monolayer graphene, dielectric engineering⁴⁶ and advanced quantum electronics⁴⁷.

METHODS

Fluorination of BLG. BLG was exfoliated from graphite (NGS Naturgraphit, Germany) on SiO₂/Si substrate. The bilayer flakes were defined from the visual contrast in an optical microscope, and verified by Raman scattering. The samples were annealed at 300 °C in Ar/H₂ environment for 2 hours to remove residues on their surfaces. Fluorination is carried out in an inductively coupled plasma etcher (ICP, SPTS Technology) using SF₆ precursor gas with a platen power of 20W at room temperature under a high vacuum of 10⁻⁶ Torr. The fluorination time was typically short (1-2 min) in attempt to primarily affect the top layer.

Fabrication of BLG and FBLG device. Metal contacts of Cr/Au (20/80 nm) were made on pristine and fluorinated bilayer graphene using standard electron-beam lithography (JEOL 9500FSZ at 100 keV) and e-beam evaporation. Back gate voltages were applied to the highly p-doped Si substrate with a 300-nm thick SiO₂ layer to make the field effect transistor structure.

Fabrication MoS₂ device with FBLG insertion layer. Multilayer MoS₂ was first mechanically exfoliated from bulk materials (HQ graphene) on an SiO₂/Si substrate. BLG was stacked on the MoS₂ flake by an aligned transfer under a microscope^{34,35}. The sample then is spin coated with PMMA, and the contact regions are opened using electron-beam lithography. Plasma fluorination is applied to induce FBLG, and metals with different work functions including Ti, Cr, Au, and Pd with a thickness of 20 nm are deposited as the electrical contacts. To protect the metals from oxidation, all the contacts are covered by a thick Au layer (100 nm).

Raman and XPS spectroscopies. Raman spectra were acquired at room temperature with an excitation wavelength of 532 nm. XPS measurements were conducted at room temperature under a high vacuum of 10⁻⁹ mbar.

Electrical characterization. Electrical transport measurement of the fabricated devices were performed using a semiconductor parameter analyzer (Keithley 2000) in a vacuum probe-station which can heat the sample state at different temperatures.

ASSOCIATED CONTENT

Supporting Information.

Supporting information includes Figures S1-S5 showing the Raman spectra of pristine and fluorinated BLG, and the transfer curve of the MoS₂ transistors fabricated with different metal contacts without and with FBLG and the extracted SBH at the metal/MoS₂ interfaces.

AUTHOR INFORMATION

Corresponding Author

Manh-Ha Doan; E-mail address: mando@dtu.dk

Peter Bøggild; E-mail address: pbog@dtu.dk

Notes

The authors declare no competing financial interest.

ACKNOWLEDGMENTS

This work was supported by the Danish National Research Foundation (DNRF) Center for Nanostructured Graphene (DNRF103) and EU Graphene Flagship Core 3 (881603). Cheng Xiang acknowledges the support from the China Scholarship Council (Grant No. 201906240046).

REFERENCES

1. Thompson, S. E.; Parthasarathy, S. Moore's Law: the Future of Si Microelectronics. *Mater. Today* **2006**, 9, 20-25.
2. Waldrop, M. M. The Chips Are Down for Moore's Law. *Nature* **2016**, 530, 144–147.
3. Liu, Y.; Duan, X.; Shin, H.-J.; Park, S.; Huang, Y.; Duan, X. Promises and Prospects of Two-dimensional Transistors. *Nature* **2021**, 591, 43-53.
4. Das, S.; Sebastian, A.; Pop, E.; McClellan, C. J.; Franklin, A. D.; Grasser, T.; Knobloch, T.; Illarionov, Y.; Penumatcha, A. V.; Appenzeller, J.; Chen, Z.; Zhu, W.; Asselberghs, I. Transistors Based on Two-dimensional Materials for Future Integrated Circuits. *Nat. Electron.* **2021**, 4, 786-799.
5. Schwierz, F. Graphene Transistors. *Nat. Nano.* **2010**, 5, 487-496.
6. Schulman, D. S.; Arnold, A. J.; Das, S. Contact Engineering for 2D Materials and Devices. *Chem. Soc. Rev.* **2018**, 47, 3037-3058.
7. Kim, C.; Moon, I.; Lee, D.; Choi, M. S.; Ahmed, F.; Nam, S.; Cho, Y.; Shin, H.-J.; Park, S.; Yoo, W. J. Fermi Level Pinning at Electrical Metal Contacts of Monolayer Molybdenum Dichalcogenides. *ACS Nano* **2017**, 11, 1588-1596.
8. Kim, G.-S.; Kim, S.-H.; Park, J.; Han, K. H.; Kim, J.; Yu, H.-Y. Schottky Barrier Height Engineering for Electrical Contacts of Multilayered MoS₂ Transistors with Reduction of Metal-Induced Gap States. *ACS Nano* **2018**, 12, 6292-6300.
9. Chen, R.-S.; Ding, G.; Zhou, Y.; Han, S.-T. Fermi-level Depinning of 2D Transition Metal Dichalcogenide Transistors. *J. Mater. Chem. C* **2021**, 9, 11407-11427.
10. Zheng, Y.; Gao, J.; Han, C.; Chen, W.; Ohmic Contact Engineering for Two-Dimensional Materials. *Cell Rep. Phys. Sci.* **2021**, 2, 100298.
11. Sze, S. M.; Ng, K. K. *Physics of Semiconductor Devices*, 3rd ed.; John Wiley & Sons: Hoboken, NJ, 2007
12. Liaoa, M.-H.; Lien, C. The Comprehensive Study and The Reduction of Contact Resistivity on the n-InGaAs M-I-S Contact System with Different Inserted Insulators. *AIP Adv.* **2015**, 5, 057117.
13. Pak, Y.; Park, W.; Mitra, S.; Devi, A. A. S.; Loganathan, K.; Kumaresan, Y.; Kim, Y.; Cho, B.; Jung, G.-Y.; Hussain, M. M.; Roqan, Iman S. Enhanced Performance of MoS₂ Photodetectors by Inserting an ALD-Processed TiO₂ Interlayer. *Small* **2018**, 14, 1703176.

14. Jang, J.; Yunseob Kim, Y.; Chee, S.-S.; Kim, H.; Whang, D.; Kim, G.-H.; Yun, S. J. Clean Interface Contact Using a ZnO Interlayer for Low-Contact-Resistance MoS₂ Transistors. *ACS Appl. Mater. Inter.* **2020**, *12*, 5031–5039.
15. Wang, J.; Yao, Q.; Huang, C. W.; Zou, X.; Liao, L.; Chen, S.; Fan, Z.; Zhang, K.; Wu, W.; Xiao, X.; Jiang, C.; Wu, W. W. High Mobility MoS₂ Transistor with Low Schottky Barrier Contact by Using Atomic Thick h-BN as a Tunneling Layer. *Adv. Mater.* **2016**, *28*, 8302–8308.
16. Nair, R. R.; Ren, W.; Jalil, R.; Riaz, I.; Kravets, V. G.; Britnell, L.; Blake, P.; Schedin, F.; Mayorov, A. S.; Yuan, S.; Katsnelson, M. I.; Cheng, H.-M.; Strupinski, W.; Bulusheva, L. G.; Okotrub, A. V.; Grigorieva, I. V.; Grigorenko, A. N.; Novoselov, K. S.; Geim, A. K. Fluorographene: A Two-Dimensional Counterpart of Teflon. *Small* **2010**, *6*, 2877–2884.
17. Son, J.; Ryu, H.; Kwon, J.; Huang, S.; Yu, J.; Xu, J.; Watanabe, K.; Taniguchi, T.; Ji, E.; Lee, S.; Shin, Y.; Kim, J. H.; Kim, K.; van der Zande, A. M.; Lee, G.-H. Tailoring Single- and Double-Sided Fluorination of Bilayer Graphene via Substrate Interactions. *Nano Lett.* **2021**, *21*, 891–898.
18. Jessen, B. S.; Whelan, P. R.; Mackenzie, D. M. A.; Luo, B.; Thomsen, J. D.; Gammelgaard, L.; Booth, T. J.; Bøggild, P. Quantitative Optical Mapping of Two-dimensional Materials. *Sci. Rep.* **2018**, *8*, 638.
19. Felten, A.; Flavel, B. S.; Britnell, L.; Eckmann, A.; Louette, P.; Pireaux, J.-J.; Hirtz, M.; Krupke, R.; Casiraghi, C. Single- and Double-Sided Chemical Functionalization of Bilayer Graphene. *Small* **2013**, *9*, 631–639.
20. Robinson, J. T.; Burgess, J. S.; Junkermeier, C. E.; Badescu, S. C.; Reinecke, T. L.; Perkins, F. K.; Zalalutdniov, M. K.; Baldwin, J. W.; Culbertson, J. C.; Sheehan, P. E.; Snow, E. S. Properties of Fluorinated Graphene Films. *Nano Lett.* **2010**, *10*, 3001–3005.
21. Danielsen, D. R.; Lyksborg-Andersen, A.; Nielsen, K. E. S.; Jessen, B. S.; Booth, T. J.; Doan, M.-H.; Zhou, Y.; Bøggild, P.; Gammelgaard, L. Super-Resolution Nanolithography of Two-Dimensional Materials by Anisotropic Etching. *ACS Appl. Mater. Interfaces* **2021**, *13*, 41886–41894.
22. Park, J.; Jo, S. B.; Yu, Y.-J.; Kim, Y.; Yang, J. W.; Lee, W. H.; Kim, H. H.; Hong, B. H.; Kim, P.; Cho, K.; Kim, K. S. Single-Gate Bandgap Opening of Bilayer Graphene by Dual Molecular Doping. *Adv. Mater.* **2012**, *24*, 407–411.

23. Zhang, W.; Lin, C.-T.; Liu, K.-K.; Tite, T.; Su, C.-Y.; Chang, C.-H.; Lee, Y.-H.; Chu, C.-W.; Wei, K.-H.; Kuo, J.-L.; Li, L.-J. Opening an Electrical Band Gap of Bilayer Graphene with Molecular Doping. *ACS Nano* **2011**, *5*, 7517-7524.
24. Ohta, T.; Bostwick, A.; Seyller, T.; Horn, K.; Rotenberg, E. Controlling the Electronic Structure of Bilayer Graphene. *Science* **2006**, *313*, 951-954.
25. Xia, F.; Farmer, D. B.; Lin, Y.-M.; Avouris, P. Graphene Field-Effect Transistors with High On/Off Current Ratio and Large Transport Band Gap at Room Temperature. *Nano Lett.* **2010**, *10*, 715-718.
26. Bakharev, P. V.; Huang, M.; Saxena, M.; Lee, S. W.; Joo, S. H.; Park, S. O.; Dong, J.; Camacho-Mojica, D. C.; Jin, S.; Kwon, Y.; Biswal, M.; Ding, F.; Kwak, S. K.; Lee, Z.; Ruoff, R. S. Chemically Induced Transformation of Chemical Vapour Deposition Grown Bilayer Graphene into Fluorinated Single-layer Diamond. *Nat. Nano.* **2020**, *15*, 59-67.
27. Feng, W.; Long, P.; Feng, Y.; Li, Y. Two-Dimensional Fluorinated Graphene: Synthesis, Structures, Properties and Applications. *Adv.Sci.* **2016**, *3*, 1500413.
28. Nourbakhsh, A.; Zubair, A.; Sajjad, R. N.; Tavakkoli, K. G. A.; Chen, W.; Fang, S.; Ling, X.; Kong, J.; Dresselhaus, M. S.; Kaxiras, E.; Berggren, K. K.; Antoniadis, D.; Palacios, T. MoS₂ Field-Effect Transistor with Sub-10 nm Channel Length. *Nano Lett.* **2016**, *16*, 12, 7798–7806.
29. Tran, M. D.; Kim, H.; Kim, J. S.; Doan, M. H.; Chau, T. K.; Vu, Q. A.; Kim, J.-H.; Lee, Y. H. Two-terminal Multibit Optical Memory via van der Waals Heterostructure. *Adv. Mater.* **2019**, *31*, 1807075.
30. Liang, S.; Yang, H.; Renucci, P.; Tao, B.; Laczkowski, P.; Mc-Murtry, S.; Wang, G.; Marie, X.; George, J.-M.; Petit-Watelot, S.; Djeflal, A.; Mangin, S.; Jaffre`s, H.; Lu, Y. Electrical Spin Injection and Detection in Molybdenum Disulfide Multilayer Channel. *Nat. Commun.* **2017**, *8*, 14947.
31. Luo, Y. K.; Xu, J.; Zhu, T.; Wu, G.; McCormick, E. J.; Zhan, W.; Neupane, M. R.; Kawakami, R. K. Opto-Valleytronic Spin Injection in Monolayer MoS₂/Few-Layer Graphene Hybrid Spin Valves. *Nano Lett.* **2017**, *17*, 3877–3883.
32. Kim, S.; Park, H.; Choo, S.; Baek, S.; Kwon, Y.; Liu, N.; Yang, J. Y.; Yang, C.-W.; Yoo, G.; Kim, S. Active-matrix Monolithic Gas Sensor Array Based on MoS₂ Thin-film Transistors. *Commun. Mater.* **2020**, *1*, 86.

33. Wang, Z.; Mi, B.; Environmental Applications of 2D Molybdenum Disulfide (MoS₂) Nanosheets. *Environ. Sci. Technol.* **2017**, 51, 8229–8244.
34. Doan, M.-H.; Jin, Y.; Adhikari, S.; Lee, S.; Zhao, J.; Lim, S. C.; Lee, Y. H.; Charge Transport in MoS₂/WSe₂ van der Waals Heterostructure with Tunable Inversion Layer. *ACS Nano* **2017**, 11, 3832–3840 .
35. Doan, M.-H.; Jin, Y.; Chau, T. K.; Joo, M.-K.; Lee, Y. H. Room-temperature Mesoscopic Fluctuations and Coulomb Drag in Multilayer WSe₂. *Adv. Mater.* **2019**, 31, 1900154.
36. Das, S.; Chen, H.-Y.; Penumatcha, A. V.; Appenzeller, J. High Performance Multilayer MoS₂ Transistors with Scandium Contacts. *Nano Lett.* **2013**, 13, 1, 100–105.
37. Cui, X.; Shih, E.-M.; Jauregui, L. A.; Chae, S. H.; Kim, Y. D.; Li, B.; Seo, D.; Pistunova, K.; Yin, J.; Park, J.-H.; Choi, H.-J.; Lee, Y. H.; Watanabe, K.; Taniguchi, T.; Kim, P.; Dean, C. R.; Hone, J. C.; Low-Temperature Ohmic Contact to Monolayer MoS₂ by van der Waals Bonded Co/h-BN Electrodes. *Nano Lett.* **2017**, 17, 4781–4786.
38. Bampoulis, P.; Bremen, R. v.; Yao, Q.; Poelsema, B.; Zandvliet, H. J. W.; Sotthewes, K.; Defect Dominated Charge Transport and Fermi Level Pinning in MoS₂/Metal Contacts. *ACS Appl. Mater. Inter.* **2017**, 9, 19278–19286.
39. Sotthewes, K.; Bremen, R. v.; Dollekamp, E.; Boulogne, T.; Nowakowski, K.; Kas, D.; Zandvliet, H. J. W.; Bampoulis, P. Universal Fermi-Level Pinning in Transition-Metal Dichalcogenides. *Phys. Chem. C* **2019**, 123, 5411–5420.
40. Liu, Y.; Guo, J.; Zhu, E.; Liao, L.; Lee, S.-J.; Ding, M.; Shakir, I.; Gambin, V.; Huang, Y.; Duan, X. Approaching the Schottky-Mott limit in van der Waals metal-semiconductor junctions. *Nature* **2018**, 557, 696-700.
41. Robertson, J. Band Offsets, Schottky Barrier Heights, and Their Effects on Electronic Devices, *J. Vac. Sci. Technol., A* **2013**, 31, 050821.
42. Lee, Y.; Bae, S.; Jang, H.; Jang, S.; Zhu, S.-E.; Sim, S. H.; Song, Y. I.; Hong, B. H.; Ahn, J.-H. Wafer-Scale Synthesis and Transfer of Graphene Films. *Nano Lett.* **2010**, 10, 490-493.
43. Nguyen, V. L.; Duong, D. L.; Lee, S. H.; Avila, J.; Han, G.; Kim, Y.-M.; Asensio, M. C.; Jeong, S.-Y.; Lee, Y. H. Layer-controlled Single-crystalline Graphene Film with Stacking Order via Cu–Si Alloy Formation. *Nat. Nano.* **2020**, 15, 861-867.

44. Wang, Q.; Li, N.; Tang, J.; Zhu, J.; Zhang, Q.; Jia, Q.; Lu, Y.; Wei, Z.; Yu, H.; Zhao, Y.; Guo, Y.; Gu, L.; Sun, G.; Yang, W.; Yang, R.; Shi, D.; Zhang, G. Wafer-Scale Highly Oriented Monolayer MoS₂ with Large Domain Sizes. *Nano Lett.* **2020**, *20*, 7193–7199.
45. Shivayogimath, A.; Whelan, P. A.; Mackenzie, D. M. A.; Luo, B.; Huang, D.; Luo, D.; Wang, M.; Gammelgaard, L.; Shi, H.; Ruoff, R. S.; Bøggild, P.; Booth, T. J. Do-It-Yourself Transfer of Large-Area Graphene Using an Office Laminator and Water. *Chem. Mater.* **2019**, *31*, 2328–2336.
46. Knobloch, T.; Illarionov, Y. Y.; Ducry, F.; Schleich, C.; Wachter, S.; Watanabe, K.; Taniguchi, T.; Mueller, T.; Walzl, M.; Lanza, M.; Vexler, M. I.; Luisier, M.; Grasser, T.; The Performance Limits of Hexagonal Boron Nitride as an Insulator for Scaled CMOS Devices Based on Two-dimensional Materials. *Nat. Electron.* **2021**, *4*, 98-108.
47. Liu, C.; Chen, H.; Wang, S.; Liu, Q.; Jiang, Y.-G.; Zhang, D. W.; Liu, M.; Zhou, P. Two-dimensional Materials for Next-generation Computing Technologies. *Nat. Nano.* **2020**, *15*, 545-557.

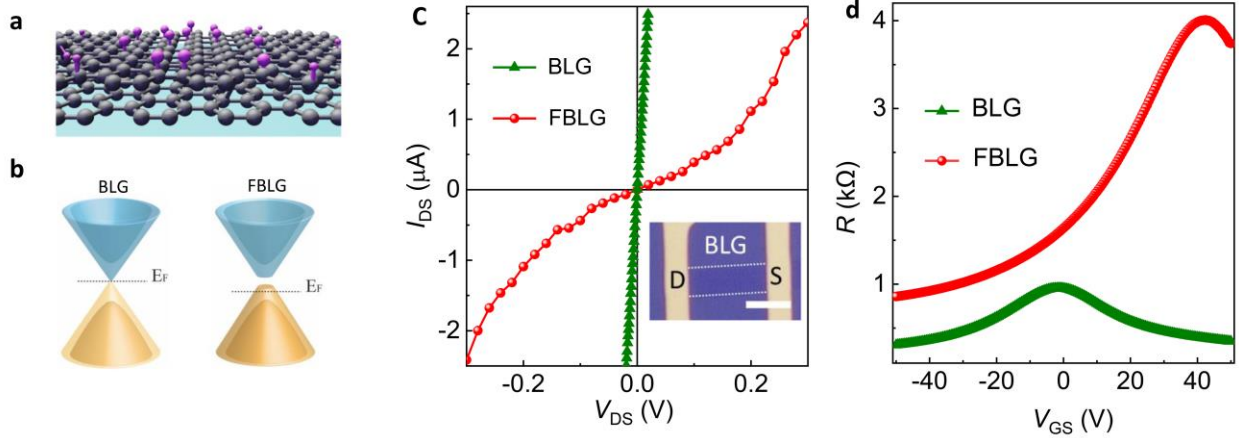


Figure 1. (a) Schematic of a cross-sectional view of FBLG on the substrate. Gray circles denote the carbon (C) atoms and the pink ones represent the fluoride (F) atoms. Covalent C-F bondings form at the surface of the top layer of BLG after fluorination. (b) Band diagram of pristine BLG and FBLG. (c) Current-voltage characteristics of BLG and FBLG at $V_G = 0$ V. The inset shows an optical microscopy image of the device. Scale bar is 5 μm . (d) Dependence of the resistivity of the BLG and FBLG on the back-gate voltage. Higher on-off ratio observed in the FBLG device suggests the presence of a band gap opening after fluorination.

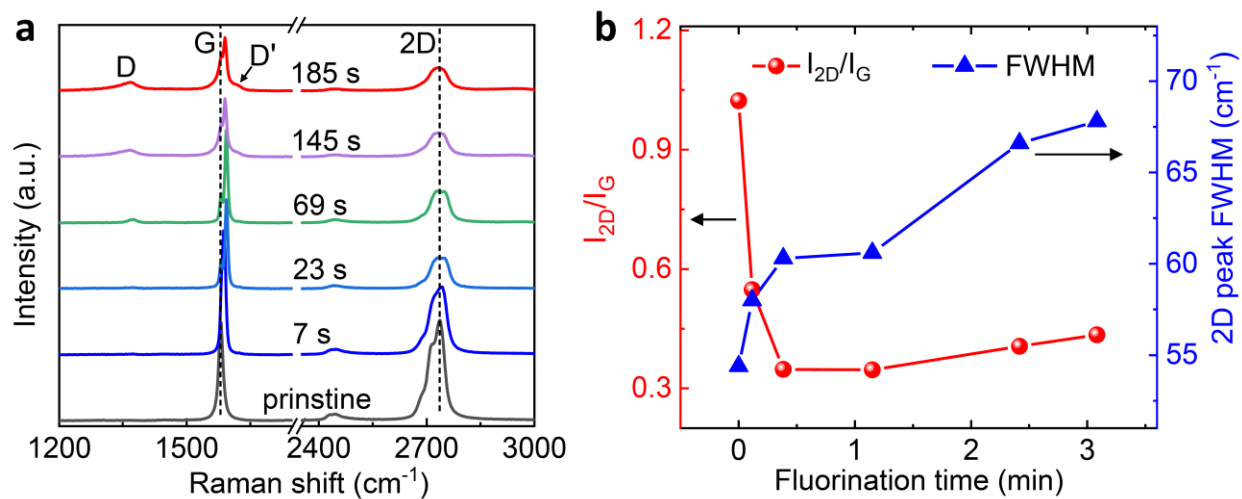


Figure 2. (a) Evolution of the Raman spectra of BLG with increasing fluorination time. (b) Intensity and full width of half-maximum (FWHM) of the 2D peak as a function of fluorination time.

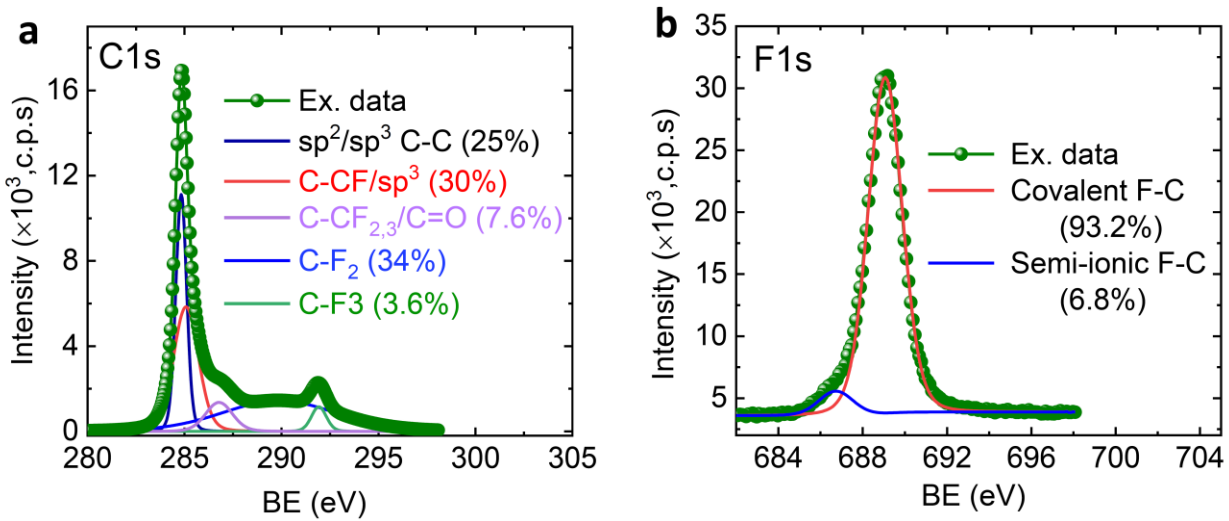


Figure 3. XPS spectra of FBLG in the (a) C1s and (b) F1s ranges.

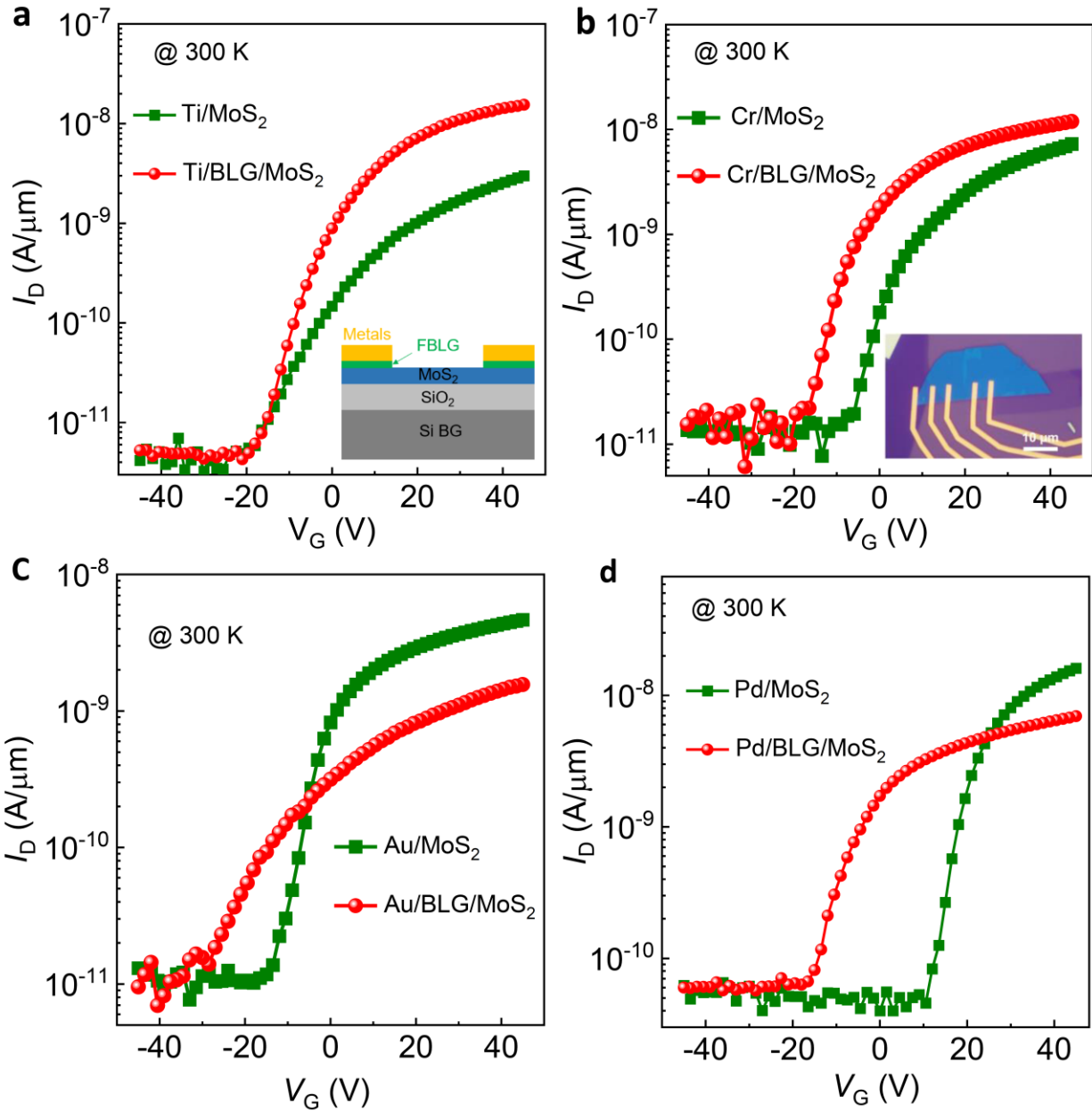


Figure 4. Transfer curves of the MoS₂ transistors without and with FBLG insertion into the metal/MoS₂ interfaces (a-d). The insets of Figure 4a and 4b show a cross-sectional schematic and the optical microscopy image of MoS₂ device.

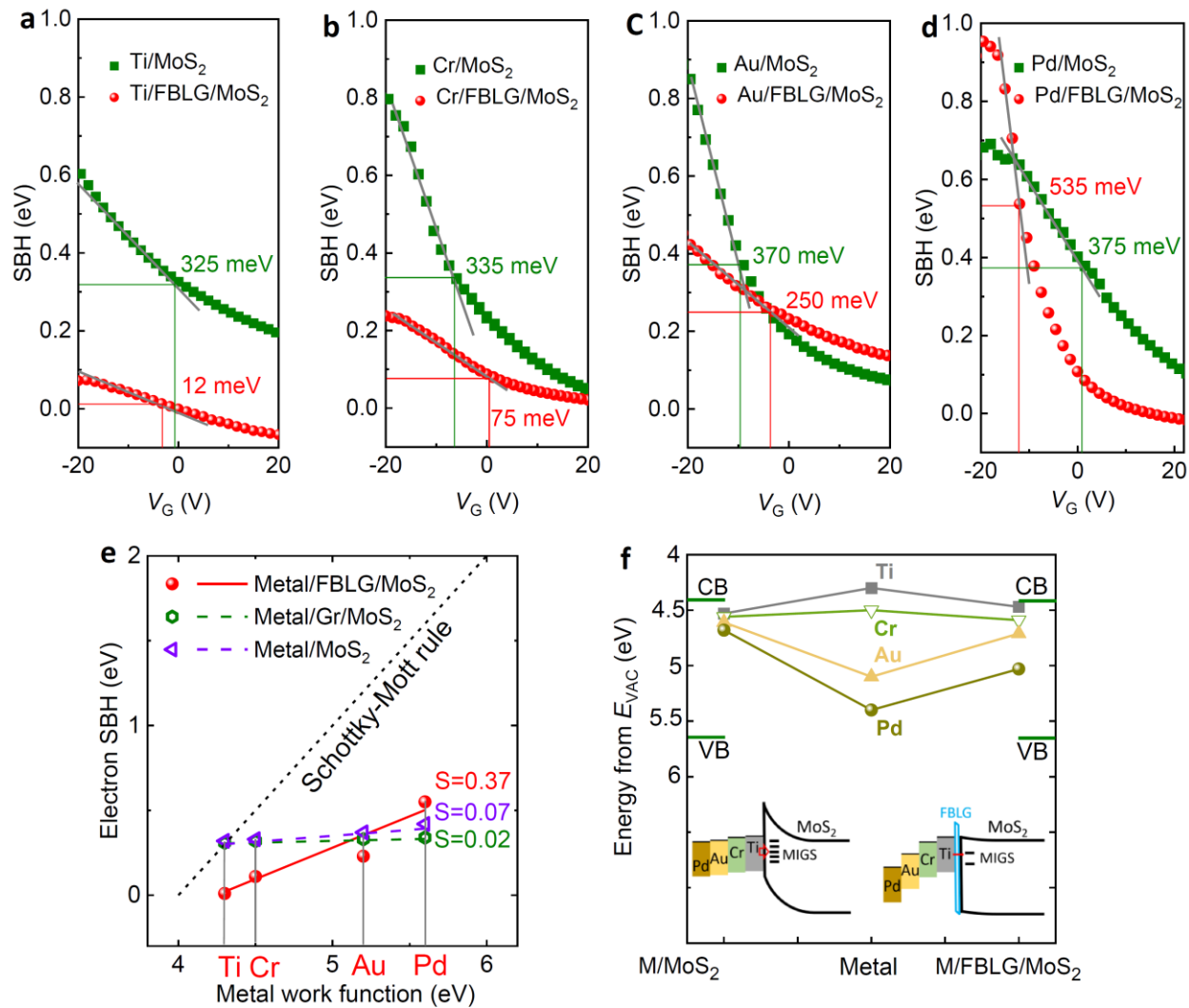


Figure 5. (a-d) Effective electron Schottky barrier height of the metal/MoS₂ contacts without and with FBLG. (e) Extracted pinning factor (S) for the MoS₂ devices with different contacts. (f) Alignment of the Fermi level in MoS₂ with the metal contacts without and with inserted FBLG.